Towards phase transferable potential functions

Jordan, Peter C.; van Maaren, Paul J.; Mavri, Janez; van der Spoel, David; Berendsen, Herman J. C.

Published in:
Journal of Chemical Physics

DOI:
10.1063/1.469703

Publication date:
1995

Towards phase transferable potential functions: Methodology and application to nitrogen

Peter C. Jordan, Paul J. van Maaren, Janez Mavri, David van der Spoel, and Herman J. C. Berendsen

Citation: The Journal of Chemical Physics **103**, 2272 (1995); doi: 10.1063/1.469703
View online: https://doi.org/10.1063/1.469703
View Table of Contents: http://aip.scitation.org/toc/jcp/103/6
Published by the American Institute of Physics

Towards phase transferable potential functions: Methodology and application to nitrogen

Peter C. Jordan,[a] Paul J. van Maaren, Janez Mavri,[b] David van der Spoel, and Herman J. C. Berendsen
Bioson Research Institute, Department of Biophysical Chemistry, University of Groningen, The Netherlands

(Received 28 November 1994; accepted 2 May 1995)

We describe a generalizable approach to the development of phase transferable effective intermolecular potentials and apply the method to the study of N_2. The method is based on a polarizable shell model description of the isolated molecule and uses experimental data to establish the parameters. Consideration of the Ne dimer shows this to be a conceptual advance over point polarizability descriptions of atomic interaction. Our parametrization of N_2 accurately describes not only the molecule's electrostatic field (i.e., a practical representation of the molecular charge distribution) but also its response to electrical and mechanical stress (polarization and deformation). The purely intermolecular terms in our potential reflect shell-shell interactions. These are parametrized by fitting properties of the low temperature solid phase of nitrogen. We derive a phase transferable potential able to account for the second virial coefficient of the gas phase, the pressure induced phase transition between nitrogen's cubic and tetragonal phases, and a wide range of liquid properties (pair distribution function, heat of vaporization, self-diffusion coefficient and dielectric constant). © *1995 American Institute of Physics.*

I. INTRODUCTION

The development of phase transferable intermolecular potentials is of great interest to computational chemists and physicists.[1] The goal is simple, computationally tractable, classical functions that reliably approximate an inherently quantum problem. Effective potentials are inherently flawed, and rely to some degree (possibly a large one) on error compensation in their application. The most familiar examples are those in common (and effective) use to describe the properties of liquid water and aqueous solutions. They treat the water molecule as a collection of fixed charges with electric moments very different from those of the isolated molecule, e.g. the dipole moment typically corresponds to the average dipole moment of bulk water.[2,3] They are parametrized to mimic behavior in liquid water and must be used with increasing caution when applied to physical systems where important aspects of water's environment differ significantly from water in bulk. Two such applications are the simulation of the water-lipid interface and of water in transmembrane ion channels. As long as a potential is applied to problems where important interactions are not substantially different from those that most greatly influence the molecular properties used in determining the parameters of the potential function, the errors in the intermolecular potential may well compensate and the simulations be in reasonable accord with experiment. The problem is that an intermolecular potential is not the sum of immutable pair (or higher) interactions; the potential energy functions themselves change depending on a molecule's surroundings. The most important of these interactions is the three-body potential, which is dominated by polarization.

We present a general approach designed to circumvent the difficulties just outlined. We first consider the electrostatic contributions and develop a quasiclassical approach that accurately describes the molecule's electrical potential and its response to electrical stress (polarization). This potential is designed to be reliable at distances well within the molecule's repulsive core; the actual value depends on the type of application envisaged. With the electrical problem solved, we seek simple functions to account for non-classical contributions due to dispersion and core repulsion between molecules. By carefully constructing the ''classical'' (coulombic and polarization) part of the potential, terms accounting for intermolecular quantum phenomena are not biased by inaccuracies in the electrical description of the molecule. *Ab initio* quantum calculations guide us in the choice of the properties to be used in constructing the molecular model. The molecular charge distribution is treated in terms of the shell model, with mobile charges bound to their respective nuclei by polarization springs. The model is parametrized from experimental data; it is not limited by the reliability of the *ab initio* quantum calculations. This approach, in which the shells (a simplified portrayal of the charge distribution) are closely coupled to the nuclei, could possibly yield potential functions in which many of the shorter range, cooperative, structural interactions (e.g. coupling between dihedral changes and bond bending) within a large molecule (e.g. a hydrocarbon or a protein) would be accounted for by the interaction between the shells. In this way we may find a relatively simple force field, rather than accounting for each modulating influence separately.[4]

We expect that if a potential adequately represents phenomena over a wide PVT domain it can be used with confidence in domains of phase space very different from those in which it has been tested. The method we present is designed to be both chemically intuitive and interpretable in terms of ''atomic'' and ''bond'' contributions. As will become evident,

[a]Permanent address: Department of Chemistry, Brandeis University, Waltham, MA 02254.
[b]Also at National Institute of Chemistry, P. O. B. 30, 61115 Ljubljana, Slovenia.

 0021-9606/95/103(6)/2272/14/$6.00

the treatment naturally requires considering deformability and the response to mechanical stress.

There is an extensive literature treating polarizable and deformable potentials, ones designed to reproduce the results of *ab initio* quantum calculations and direct quantum simulation of many particle systems. Limiting illustration to recent studies of water, approaches run the gamut from developing potential functions that attempt to accommodate dissociation phenomena,[5] that parametrize an *ab initio* water-water potential energy computation,[6] that parametrize to accommodate an extensive array of thermodynamic and spectroscopic data[7] and finally that present a Car-Parrinello[8] study of a box of 32 water molecules.[9]

We use the shell model[10] which is electrostatically equivalent to treating polarizability as a point site property.[11–13] However, it is a more flexible method. The shells, approximating mobile valence electron distributions, need not be point charges. Complex charge distributions and molecular deformability are naturally incorporated; introducing a single polarizability alters the molecular charge distribution, not just one electrical moment. The shell model lends itself readily to accounting for dissociation and for both hyper- and higher polarizabilities.[14] It can provide a basis for simpler, computationally less demanding approximations.

We first consider rare gas dimers and show that, when extended to account for non-classical interactions, a shell model treatment is conceptually superior to a point polarizability one. We then extend the analysis to homonuclear diatomic molecules, consider N_2, and develop a shell model that accurately describes the molecule's electrical properties to within 0.3 nm of either atomic center. With this molecular model, we fit the strictly intermolecular contributions to the potential to properties of the low temperature solid, the cubic α-phase. We compute the second virial coefficient, and find the potential is phase transferable. We apply the model to the γ-phase of the solid and the liquid. Our potential accounts for the α to γ phase transition for a wide range of properties of the liquid. Finally we compare our results with those determined *ab initio* and discuss possible future applications.

II. THE SHELL MODEL FOR INERT GASES

Shell model potentials are more computer intensive than those using point polarizabilities. To demonstrate that they can better approximate reality consider an elementary application, interacting inert gas atoms. Each nucleus has a charge $+q$. It is surrounded by a spherical shell of compensating charge displaced by $\mathbf{r}$, bound by a Hooke's law spring of force constant $1/\alpha$, (α is the atomic polarizability[10]). The polarization potential energy, U_{pol}, is

$$U_{\mathrm{pol}}=(q\mathbf{r})^2/2\alpha=\boldsymbol{\mu}^2/2\alpha. \tag{1}$$

This description of the isolated atom is equivalent to a point polarizability treatment.[11–13]

In addition to Eq. (1), there is a coulombic term U_{coul}. Charges coupled by means of "polarization springs" do not interact electrostatically. In the low energy configuration the system is collinear so that, at an internuclear separation R, the coulomb energy is

$$U_{\mathrm{coul}}=q^2[R^{-1}-(R+r_1)^{-1}-(R-r_2)^{-1}+(R+r_1-r_2)^{-1}]. \tag{2}$$

Because shells are mobile, there are dispersion forces between the atoms; the dimer develops an instantaneous quadrupole moment for non-zero shell displacements.[12] However, considering only coulombic and polarization energy provides a classical description of the interaction between inert gas atoms. The stable solution at any R is $r_1=r_2=0$. In the classical shell model at 0 K dispersion forces vanish and the equilibrium dimer has no quadrupole moment.[12]

What is missing? Fundamental intrinsic quantum mechanical features of interatomic interaction have been neglected. The shells are not simply point charges connected to the nuclei by springs. They represent approximate descriptions of the mobile parts of the electron clouds surrounding the nuclei. The coulomb potential, Eq. (2), neglects exchange, dispersion, the repulsive core and shielding. How can these limitations be circumvented? One possibility is to develop a quantum analog of the shell model.[15] For simplicity, and to parametrize our models from experimental data, we choose a different approach, and introduce an ansatz to account for neglected effects. Our rationale is twofold: we wish to exploit well established conventional molecular modeling software; molecular properties are still generally more reliably determined from experiment than from *ab initio* quantum calculations.

For the inert gas dimer, shielding can be ignored unless R is very small. If the shell distribution is $2p$-like Slater's rules[16] indicate that at Ne-Ne separations > 0.25 nm, shielding is totally negligible. To correct for "missing terms" and treat shell charge interaction, we augment the Hamiltonian by introducing a non-classical term, U_{nc}, describing core repulsion and London dispersion energy. Only one feature of U_{nc} is material in treating inert gas dimers: its leading term at large interparticle separations is proportional to R^{-6}. The dimer's total potential energy is

$$U_{\mathrm{shell}}=U_{\mathrm{pol}}+U_{\mathrm{coul}}+U_{\mathrm{nc}}. \tag{3}$$

The energy is determined by minimizing U_{shell} with respect to the shell variables r_1 and r_2; electronic motion is treated in an adiabatic approximation. As quantum mechanical interactions describe electronic phenomena, we choose U_{nc} to be a function of the *intershell distance* $R+r_1-r_2$. Because there is no external electric field, all charges lie on a line and $r_1=-r_2=\xi R$. Since ξ is small the result is

$$\xi=\frac{\gamma}{1+2\gamma}\frac{R}{q^2}\frac{dU_{\mathrm{nc}}}{d\ \ln R} \tag{4}$$

where $\gamma=\alpha/R^3$. The dimer's *ground state* quadrupole moment, M_4, is

$$M_4=qR^2\xi(1+\xi)\rightarrow\frac{R\alpha}{q}\frac{dU_{\mathrm{nc}}}{dR} \tag{5}$$

and its energy is U_{nc}; the correction introduced by the "classical" terms, $U_{\mathrm{pol}}+U_{\mathrm{coul}}$, is $\sim(\xi R)^2$ and negligible, $O(R^{-14})$. We expect that non-classical effects reflect shell-shell interactions and depend on the intershell distance. Functional dependence on internuclear distance can be rigor-

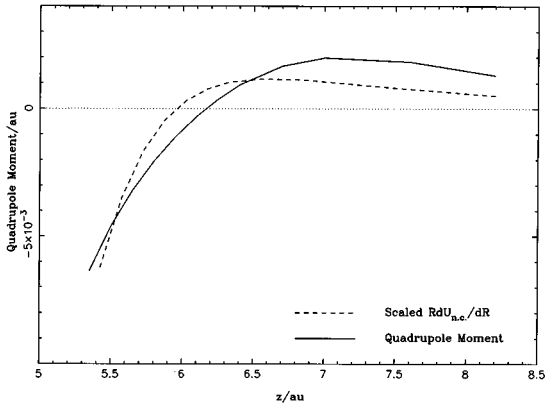

FIG. 1. Test of the shell model expression [Eq. (5)] relating the quadrupole moment of the Ne_2 dimer to the interatomic force. The data are those determined from Woon's (Refs. 18, 20) calculations based on an aug-cc-pVQZ basis set. The best fit is for a Ne shell charge of 0.6 e_o.

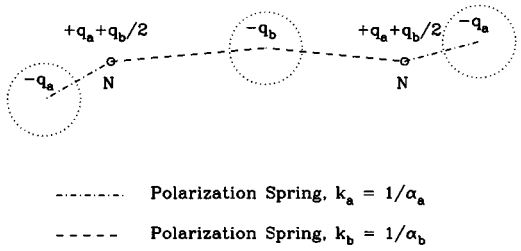

FIG. 2. Shell model for diatomic molecules. Atomic shells of charge q_a are bound to fixed nuclei of compensating charge by a polarization spring of strength $1/\alpha_a$. The mobile nuclei are connected by polarization springs of strength α_b to a bond shell of charge $-q_b$. The compensating nuclear charge is $+q_a+q_b/2$. All charges not directly linked by polarization springs interact electrostatically. The shells are *not* point charges; thus there may be shielding of the coulombic interactions (see the text); the shell radii correspond to the decay length of the charge density, using Slater's rules as a guide. In addition "non-classical" interactions between the shells are introduced to account for quantum phenomena (see the text).

ously excluded since then $\xi=0$, i.e., $M_4=0$. Dependence on shell-other nucleus separation leads to results identical to those based on our original assumption, but it does not seem as "natural" to us.

In contrast to a point polarizability treatment, the shell model, *augmented to account for core repulsion and London dispersion forces*, allows rare gas dimers to develop a quadrupole moment. It predicts a precise relationship between the binding energy of the dimer, $U_{\rm nc}$ and the quadrupole moment M_4. M_4 should be proportional to the (negative) force between the atoms; as such M_4 is positive for large R, negative when R is small and zero at the minimum in the binding energy. This is certainly qualitatively reasonable. At large internuclear separations the electrons of each inert gas atom are attracted by the other nucleus, increasing the interatomic negative charge density. As the atoms approach one another closely, electron repulsion must dominate and charge is expelled from the interatomic domain.

Quantitative corroboration relies on computing the binding energy of rare gas dimers. This requires calculations beyond the Hartree-Fock (HF) level of theory (for applications to binding in Ne_2, see Refs. 17, 18) and making counterpoise corrections for basis set superposition error (BSSE).[19] Only correlated wave functions, corrected for BSSE, yield realistic binding energy curves. There is no rigorous theory for making analogous corrections to the quadrupole moment. However, very high quality quantum mechanical computations, with correlated wave functions employing very large one electron basis sets, become ever less dependent on the counterpoise correction as the basis set is improved.[18] These wave functions yield estimates of the quadrupole moment. Our qualitative picture is corroborated. The data[20] are presented in Figure 1 and yield a shell charge of $0.6e_o$; M_4 behaves as expected. Small differences between the shell model and quantum theory are not surprising. There is still noticeable BSSE, even using an aug-cc-pVQZ basis set.[18] Thus there remain uncertainties in the binding energy as well as the wave function; $RdU_{\rm nc}/{\rm dR}$ is sensitive to the former and M_4 to the latter.

The computed shell charge of $0.6e_o$ seems small, at least if identified with neon's effective charge, $\sim 5.85e_o$ from Slater's rules.[16] To determine if $0.6e_o$ is reasonable, we calculated the polarization energy of an atom interacting with a test charge Q. As long as the test charge does not approach the nucleus too closely, we find

$$W=-[Q^2\alpha/2R^4][1+2Q\alpha/qR^3+\cdots]; \tag{6}$$

there is an additional, R^{-7}, term in the energy. This prediction, using the shell charge of $0.6e_o$, was quantitatively compared with the polarization energy of Ne computed at the MP4 level using GAUSSIAN 90[21] with a 6-31g(2df) basis set. For $Q\leqslant e_o$, the differences between the two computations were <0.4 kJ/mol at all ion-atom separations $\geqslant 0.2$ nm. Even with Q as large as $1.5e_o$, where hyper- and higher polarizability may contribute, the differences were still $<$ 0.4 kJ/mol for separations $\geqslant 0.25$ nm.

III. SHELL MODEL DESCRIPTIONS OF DIATOMIC MOLECULES

The modified shell model is an improvement over a point polarizability treatment of inert gas atoms. To see if molecules can be described similarly, we consider homonuclear diatomics. In the simplest shell model the nuclei are separated by a fixed distance R. Each carries an effective charge $+q$ and has associated with it a compensating displaced shell of negative charge. In addition to the diatomic analogs of Eqs. (1) to (3), we include an electric field dependent term, $U_{\rm field}$,

$$U_{\rm field}=q(\mathbf{r}_1-\mathbf{r}_2)\cdot\mathbf{E}; \tag{7}$$

here the $\mathbf{r}_i$ are the displacements of the shells from their respective nuclei. This model can account for a diatomic's basic electrical properties: the quadrupole moment M_4 and the two polarizabilities, $\alpha_\parallel$ and $\alpha_\perp$. But it has an unattractive consequence. To describe molecules like H_2 and F_2 with positive quadrupole moments, requires a negative nuclear charge q. The mobile shells must then be positively charged holes, contradicting out basic assumption, that the shells correspond to electronic charge density.

We were thus led to the model illustrated in Figure 2. It

TABLE I. Data sets and corresponding shell model parameters for *ab initio* (AI) and Experimental (Exp) N_2.

Data sets						
Type	$\alpha_\parallel$/Å^3	$\alpha_\perp$/Å^3	M_4/(esu Å^2)	M_{16}/(esu Å^4)	R_o/Å	k_{vib}/(N m^{-1})
AI[a]	1.94	1.08	−1.35	−2.82	1.071	3097.0
Expt.[b]	2.204	1.508	−1.40	−3.5	1.097	2293.0

Shell model parameters							
Type	α_a/Å^3	α_b/Å^3	q_a/e_o	q_b/e_o	z_{eq}/Å	w_1/Å^{-2}	w_2/Å^{-3}
AI[a]	0.40367	0.42704	−2.15049	−2.40855	0.18056	1.09707	−4.96328
Expt.[b]	0.46518	0.71805	−1.31440	−2.49737	0.28669	0.76183	−3.03372

[a]*Ab initio*, MP2/6-31g(2df), calculations of properties.
[b]Experimentally determined properties, see Refs. 14, 22, 23.

has three shell charges, one associated with each atom and a third corresponding to the charge distribution in the internuclear space. The picture is intuitive: atomic shells are associated with each atom and a bond shell associated with the bond. The model has four electrical parameters, shell charges $-q_a$ and $-q_b$ and polarizabilities α_a and α_b; the subscripts "a" and "b" refer to the atomic and bond charge shells respectively. $\mathbf{r}_1$ and $\mathbf{r}_2$ are the displacements of the atomic shells from their respective nuclei, $\mathbf{r}_0$ is the displacement of the bond shell from the midpoint of the bond, which is zero for homonuclear diatomic molecules in the absence of an electric field, and $\mathbf{S}$ is one-half the bond length $\mathbf{R}$. If the equilibrium displacement of the atomic shell is z, the molecule's quadrupole moment is

$$M_4 = q_b S^2 - 2q_a z(R+z), \tag{8}$$

which can be either positive or negative while maintaining negatively charged shells. There are four terms in the potential,

$$U_{\text{shell}} = U_{\text{pol}} + U_{\text{coul}} + U_{\text{nc}} + U_{\text{field}}. \tag{9}$$

Each nucleus has a charge of $q_{\text{nucl}} = (q_a + q_b/2)$. The individual terms are

$$U_{\text{pol}} = q_a^2[\mathbf{r}_1^2 + \mathbf{r}_2^2]/2\alpha_a + q_b^2[(\mathbf{S}+\mathbf{r}_0)^2 + (\mathbf{S}-\mathbf{r}_0)^2]/2\alpha_b$$
$$= q_a^2[\mathbf{r}_1^2 + \mathbf{r}_2^2]/2\alpha_a + q_b^2[\mathbf{S}^2 + \mathbf{r}_0^2]/\alpha_b \tag{10}$$

$$U_{\text{coul}} = q_{\text{nucl}}^2/R - q_a q_{\text{nucl}}[|\mathbf{R}-\mathbf{r}_1|^{-1} + |\mathbf{R}+\mathbf{r}_2|^{-1}] + q_a^2|\mathbf{R}-\mathbf{r}_1 + \mathbf{r}_2|^{-1} + q_a q_b[|\mathbf{S}+\mathbf{r}_0-\mathbf{r}_1|^{-1} + |\mathbf{S}-\mathbf{r}_0+\mathbf{r}_2|^{-1}] \tag{11}$$

$$U_{\text{nc}} = q_a q_{\text{nucl}}[(1-f_{\text{shld}}(|\mathbf{R}-\mathbf{r}_1|))/|\mathbf{R}-\mathbf{r}_1| + (1-f_{\text{shld}}(|\mathbf{R} + \mathbf{r}_2|))/|\mathbf{R}+\mathbf{r}_2|] + q_a q_b[w_{a-b}(|\mathbf{S}-\mathbf{r}_0+\mathbf{r}_2|) + w_{a-b}(|\mathbf{S}+\mathbf{r}_1-\mathbf{r}_0|)] + q_a^2 v_{a-a}(|\mathbf{R}-\mathbf{r}_1+\mathbf{r}_2|) \tag{12}$$

$$U_{\text{field}} = \mathbf{E}\cdot[q_a(\mathbf{r}_1-\mathbf{r}_2) + q_b\mathbf{r}_0]. \tag{13}$$

U_{nc} depends on three unknown functions, f_{shld}, w_{a-b} and v_{a-a}. The first of these describes the shielding of the shell charge distribution associated with one atom by the other nucleus; it approaches 1 at large separations. The second and third terms describe non-classical interactions between the atom and bond shell charge distributions and the atom shell charge distributions respectively. In practice Eq. (12) can be greatly simplified; at least for N_2, molecular properties can be accurately described if $f_{\text{shld}} \equiv 1$ and $v_{a-a} \equiv 0$.

The model defined by Eq. (9) with Eqs. (10)–(13) is complicated but attractive. It incorporates structural change (bond stretching) as well as polarization. In addition to fitting $M_4, \alpha_\parallel$ and $\alpha_\perp$, it can also account for the equilibrium bond length R_o and the force constant, k_{vib}. As it has more than five parameters, simplification of U_{nc} is needed. Focussing on N_2, we assume that: i) the shell-other nucleus distance is large enough for shielding to be neglected, i.e. $f_{\text{shld}} \equiv 1$; ii) the separation of the atomic shells is large enough that we can ignore their non-classical interaction, i.e. $v_{a-a} \equiv 0$. All "non-classical" interactions are incorporated in the function w_{a-b}. It is not possible to completely determine its functional behavior; we only require w's first few derivatives. The shell energy is minimized with respect to the zero field shell displacement, z. To determine the first two derivatives of w_{a-b}, w_1 and w_2, introduces six parameters as well as z_{eq}, the equilibrium value of z in the isolated shell molecule. The parameter set remains underdetermined. Another constraint is needed. The final condition is that the shell model molecule reproduce the electrostatic potential $\psi(\mathbf{r}_{\text{nit}})$ surrounding the N_2 molecule at physically relevant separations $\mathbf{r}_{\text{nit}}$ from the molecular center. To treat the behavior of molecules in condensed or vapor phases, requires an accurate electrostatic potential at all values of $\mathbf{r}_{\text{nit}}$ *except* those where *inter*molecular core repulsions are large.

The set of equations needed to establish z and the basic molecular data set $\alpha_\parallel, \alpha_\perp, M_4, R_o$ and k_{vib} is summarized in Appendix A. Unlike the five molecular quantities,[14,22] of which even the electrical variables are known with considerable accuracy, $\psi(\mathbf{r}_{\text{nit}})$ cannot be accurately measured. The equations determine sets of model parameters $q_a, q_b, \alpha_a, \alpha_b, w_1$ and w_2 consistent with the basic molecular data set; if one member is given, the others are fixed. The problem is to choose among these sets. For N_2 the range of possibilities is extensive; q_b ranges between $-0.8e_o$ and $-4.0e_o$, hardly limiting. However, the hexadecapole moment M_{16} is known,[23,24] although not with the certainty of the basic molecular data set. It provides a sixth molecular property and permits us to discriminate.

To test this approach, we carried out an *ab initio* study of N_2, using GAUSSIAN-90[21] at the MP2/6-31g(2df) level of

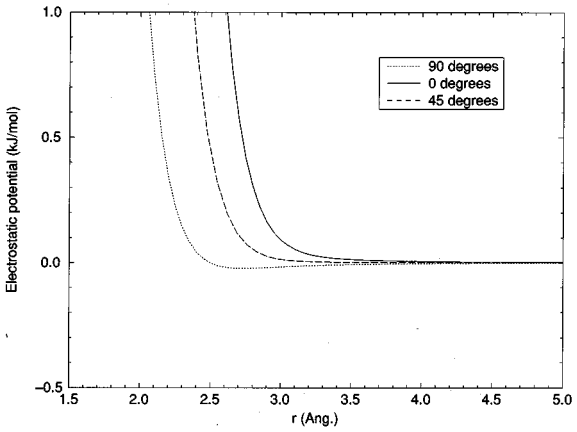

FIG. 3. Difference between molecular electrostatic potential $e_o\psi$ as computed from a N_2 Hartree-Fock wave function and from the corresponding shell model potential constructed to fit a restricted set of properties of this quantum mechanical N_2 (see the text). Three orientations are illustrated, along the molecular axis (0°), perpendicular to the bisector of the bond (90°) and along the diagonal at 45°.

theory. This yields a complete six member quantum mechanical data set from which to determine shell parameters. The quantum data set and the shell model parameters are listed in Table I. Figure 3 demonstrates that the shell model accounts for quantum mechanical N_2's electrical potential ψ exceptionally well. Regardless of the angle of approach, the difference between the shell model $e_o\psi$ and the exact result is less than 0.1 kJ/mol to within 0.28 nm of the midpoint of the bond. Since most intermolecular potentials indicate that the radius of nitrogen's repulsive core (a practical measure is pair interaction energies >4000 K) is $\sim 0.28-0.3$ nm,[25–28] the shell model accurately describes the electrical potential at distances substantially less than those sampled thermally. As important as the static potential is the polarization potential due to interaction with a test charge, q_{test}. HF/6-31g(2df) calculations for N_2 were carried out within the GAUSSIAN-90 framework for a test charge approaching the molecule either along the axis or along the bond bisector (perpendicular); illustrative data are presented in Table II. For $|q_{\text{test}}| < 0.1e_o$, there is no difference between quantum mechanical and shell model polarization potentials for all test charge-molecular origin separations $\geqslant 0.3$ nm. As the magnitude of the test charge is increased, the harmonic spring model for polarization becomes inadequate; both hyperpolarization and the higher polarizabilities[14] may be significant. However, even for $|q_{\text{test}}| = 0.5e_o$, the maximum error within the 0.3 nm envelope is 0.75 kJ/mol. The perturbation introduced by a full e_o is too large for our model to be quantitatively reliable. However, important qualitative features of the quantum mechanical result are reproduced by the shell model even when $|q_{\text{test}}| = e_o$. For a positive charge approaching perpendicular to the bond both potentials change sign at ~ 0.4 nm; the maximum in both occurs at separations $>$ 0.5 nm. Similarly, for a negative charge approaching axially, both potentials change sign at ~ 0.36 nm and exhibit maxima near ~ 0.5 nm. The largest errors are for positive charges approaching axially. For two interacting nitrogen molecules, these are configurations in which intermolecular repulsion is significant at distances as large as 0.35–0.4 nm;[27,28] thus adverse consequences for *inter*molecular modeling are reduced. Our *intra*molecular modeling procedure accomplishes a major goal: *accurately describing a molecule's electrical potential and its response to electrical stress even quite close to the molecular center.*

Table I also lists the experimental data set and the corresponding shell model parameters for N_2. Our choices for $\alpha_\parallel, \alpha_\perp$ and M_4 correspond to the best recent determinations; the uncertainty in these numbers is $\sim 5\%$.[14] M_{16} is a matter of controversy; literature values differ by $\sim 25\%$.[23,24] Measurements are based on analysis of collision induced infrared absorption and depend on assumptions about the N_2-N_2 potential function. Quantum calculations[29–32] tend to favor the lower value of M_{16}.[24] We chose the higher value[23] because that work proved better able to correlate the temperature dependent absorption. The shell model electrical potential is fairly sensitive to the value of M_{16}; changing it by 25% begins to affect $e_o\psi$ noticeably at distances $\leqslant$ 0.3 nm from

TABLE II. Tests of shell model polarization potential.

	Axial approach				Perpendicular approach			
q_{test}/e_0	$d_{0.1}$ [a]	$d_{0.5}$ [a]	$e_o\Delta\psi_{0.3\text{ nm}}$ [b]	$e_o\psi_{0.3\text{ nm}}$ [c]	$d_{0.1}$ [a]	$d_{0.5}$ [a]	$e_o\Delta\psi_{0.3\text{ nm}}$ [b]	$e_o\psi_{0.3\text{ nm}}$ [c]
+0.1	<0.30		−0.03	−2.03	<0.30		+0.01	+0.53
+0.5	0.41	0.32	−0.75	−14.69	0.36	<0.30	+0.28	+0.74
+1.0	0.50	0.41	−5.31	−41.27	0.43	0.34	+1.10	−3.11
−0.1	<0.30		−0.01	+1.58	<0.30		+0.01	−0.69
−0.5	0.37	<0.30	−0.28	+3.54	0.35	<0.30	+0.29	−5.27
−1.0	0.46	0.34	−0.82	−3.43	0.45	0.35	+1.20	−14.99

[a] $d_{0.1}$ and $d_{0.5}$ are the distances (in nm) between the test charge and the molecular origin at which the error in the shell model polarization potential is equal to 0.1 and 0.5 kJ/mol respectively.

[b] $\Delta\psi_{0.3\text{ nm}}$ is the difference between the shell model and an *ab inito* HF/6-31g(2df) calculation of the interaction energy between an N_2 molecule and a point charge, $q_{\text{test}}e_0$. This interaction energy (polarization potential) thus corresponds to the electrostatic and polarization energies in the context of the Kitaura-Morokuma (Ref. 65) energy decomposition analysis. The data describe a test charge 0.3 nm from the molecular origin; $e_0\psi$ is in kJ/mol.

[c] $\psi_{0.3\text{ nm}}$ is the *ab initio* HF/6-31g(2df) polarization potential (see footnote b) for a test charge 0.3 nm from the molecular origin; $e_0\psi$ is in kJ/mol.

the molecular origin. The energy differences are greater than 0.5 kJ/mol.

The model parameters are reasonable. The nuclear charge is $\sim+2.6e_o$; shells behave as if there has been significant screening of the nuclear charges. Slater's rules[16] suggest a comparable value, an effective charge of $\sim 3.9e_o$. The quantity $(\alpha_a+\alpha_b)$, the polarizability of each atomic center, is ~ 1.18 Å^3; the polarizability of atomic nitrogen is comparable, ~ 1.1 Å^3.[33,34] The parameters w_1 and w_2 are the first and second derivatives of the interaction potential, w_{a-b}, describing the non-coulombic coupling between the atomic and bond shells. They have a physically intuitive interpretation: i) w_1 is positive—polarizability springs do not account for all binding interactions in the nitrogen molecule; ii) w_2 is negative—binding due to interaction of the ''bond'' and ''atomic'' shells becomes weaker as their separation increases.

Finally, consider the assumptions, $f_{\text{shld}}\equiv 1$ and $v_{a-a}\equiv 0$. For our model, the shell-other nucleus distance is $\sim$ 0.13 nm; assuming the atomic shell electrons are ''2p'' in nature and can be described by Slater type 2*p*-orbitals with an effective charge given by Slater's rules, $f_{\text{shld}}=0.995$; the neglect of shielding is essentially exact. The distance between the atomic shells is $\sim$ 0.16 nm while that between atomic and bond shells is only $\sim$ 0.08 nm; thus quantum effects due to atom shell interactions are much smaller than those due to the atom-bond shell coupling. A rough quantitative measure is given by noting that the coulomb and exchange interactions are related to the square of the overlap; for Slater type 2*p*-orbitals at $\sim$ 0.16 nm separation the overlap is $\sim 30\%$ that at a separation of $\sim$ 0.08 nm, corresponding to a factor of >10 in the interaction energies.

Viewed from the perspective of the atomic sites our potential functions, based on interactions between shells, are fundamentally anisotropic. Thus they account for orientationally dependent interactions in ways that isotropic atom site-atom site terms cannot. They may thus be as effective as anisotropic atom-atom potentials,[35] but be much simpler to work with.

IV. SHELL MODEL POTENTIAL, INTERMOLECULAR CONTRIBUTIONS—THE CUBIC α-PHASE

Our model of molecular nitrogen accurately describes both the electrostatic potential and, if the test charge is not too strong, the polarization potential. Using it to model a charged complex, e.g. Na^+ solvated by N_2, would be questionable. However, for interacting N_2 molecules, where the leading term involves the quadrupolar coupling, the model should be adequate. We assume that the remaining intermolecular interactions, representing core and dispersive contributions to the potential function, are pair-wise additive. The molecular model has five force centers, of three different types: the two atomic shells, the two nuclei and the bond shell. The six types of interaction that could complete the intermolecular potential are summarized in Table III. We expect the most important contributors are the various shell-shell terms. However, we test the consequences of all six possibilities. For simplicity we assume that these terms depend only on the *distance*, R, between the interaction sites on different molecules. For computational reasons we limit consideration to the three parameter, Buckingham like exp-6, W_{BUCK}, potential

TABLE III. Interaction types for short-range intermolecular shell terms.

Type	Interaction sites
I	bond shell$_1$, bond shell$_2$
II	bond shell$_1$, atomic shells$_2$ & bond shell$_2$, atomic shells$_1$
III	atomic shells$_1$, atomic shells$_2$
IV	nuclei$_1$, bond shell$_2$ & nuclei$_2$, bond shell$_1$
V	nuclei$_1$, atomic shells$_2$ & nuclei$_2$, atomic shells$_1$
VI	nuclei$_1$, nuclei$_2$

$$W_{\text{BUCK}}=\frac{\epsilon}{(1-6/\alpha)}[(6/\alpha)\exp\{\alpha(1-R/\sigma)\}-(\sigma/R)^6]. \tag{14}$$

The ''non-classical'' terms in the intermolecular potential may depend on up to eighteen parameters if interactions involved all six possible site types. We consider each type separately and determine the corresponding parameter sets. These parameters are determined from properties of nitrogen's low temperature, low pressure cubic α-phase: its structure and density, its heat of sublimation at 0 K, and its compressibility. As only energy minimizations are required, we can rapidly scan large regions of parameter space and test a wide range of possibilities.

The crystal structure is either exactly ordered cubic (space group $Pa3$),[36] or very slightly distorted (space group $P2_13$).[37] Because any distortion is small we treat this phase as ordered cubic with four molecules per unit cell and each of the four molecular sublattices oriented along one of the four distinct threefold symmetry axes. The shell model molecule remains a linear quadrupole. The lattice parameter, a, is 0.5649 nm.[36,38] The compressibility, extrapolated to 0 K, is 47.6×10^{-6} atm^{-1}.[39] The experimental heat of sublimation at 0 K, ΔH^o_{sub}, is 6.91 kJ/mol, derived from the heat of vaporization and the heat capacities and heats of transition of nitrogen liquid and its various solid phases.[40,41] Since our intermolecular potential is an adiabatic approximation not accounting for zero point fluctuations, the enthalpy must be corrected for the zero point energy of the lattice at the center of the Brillouin zone and any shift in the molecular stretching frequency due to condensation. Excluding long wave length compression modes, there are 21 translational and librational modes of which 17 are collective;[40,42] the other four correspond to stretching of N_2. Their influence is significant, 1.34 kJ/mol;[43] the corrected heat of sublimation is $\Delta H_{\text{sub}}=8.25$ kJ/mol. The shell model permits us to directly account for the shift in the stretching frequency due to condensation and compare our model results with the experimental value, a redshift of 28 cm^{-1} (Ref. 44) from the gas phase ω_e.

In order to compute enthalpy, unit cell volume and compressibility, we compute the energy per particle, W, by placing one molecule at the origin.

$$W=\delta U_{\text{shell}}(r,S)+\sum_N \sum_B V_{0,B}(r,S,\mathbf{R}_{0,B}), \tag{15}$$

where r is the atomic shell displacement, S one half the bond length, N is the Nth coordination shell and $\mathbf{R}_{0,B}$ the vector separation of molecule ''B'' in the Nth shell from the molecule at the origin. Because of interaction with other molecules in the lattice, both r and S are shifted from those in the isolated molecule. The coordinate shells, located on concentric spheres, are defined by the indices (i,j,k), which for a cubic lattice are: $(2l,2m,2n)$, $(2l+1,2m+1,2n)$, $(2l+1,2m,2n+1)$ and $(2l,2m+1,2n+1)$ so that $N=(i^2+j^2+k^2)/2$. δU_{shell} is the shell excitation energy relative to the isolated shell molecule and $V_{0,B}$ is the total interaction energy between the molecule at the origin and that at site B, including the contribution due to the electrostatic interaction between the shell molecules and the ''non-classical'' terms. The shell excitation energy requires evaluating w_{a-b}; however we have only determined its first two derivatives. We approximate it by a Taylor series expansion about d_o (the equilibrium atom shell-bond shell separation in the isolated molecule) and keep the first three terms,

$$w_{a-b}(r)=w_0+w_1(r-d_0)+w_2(r-d_0)^2/2,$$
$$d_0=R_0/2+z_{\text{eq}}, \tag{16}$$

where z_{eq} is the equilibrium atomic shell displacement in an isolated nitrogen molecule (see Table I); as only energy differences with respect to the isolated molecule matter, all results are independent of w_0. To evaluate Eq. (15), the summation is decomposed into two terms: a direct numerical summation of all contributions due to interaction with molecules in the first N_c coordination shells; an approximate determination of the interaction energy with the more distant molecules. Since the cutoff distance for the numerical summation is chosen to be at least 1.0 nm, computation of the long-range correction was simplified by the following assumptions: the electrostatic contribution from the molecular shells is purely quadrupolar (details of the shell structure are irrelevant); only the R^{-6} parts of the intermolecular potential contribute and these can be translated from the interaction site to the molecular origin. The details are given in Appendix B. The thermodynamic energy E is determined by minimizing W with respect to both the position of the atomic shells (because the environment has quadrupolar symmetry, the bond shell remains at the molecular origin) and the internuclear separation. The pressure and compressibility, κ, are given by

$$p=-dE/dv=-(4/3a^2)dE/da, \quad v=V/N=a^3/4, \tag{17}$$

$$\kappa^{-1}=v\,d^2E/dv^2=[(4/9a)d^2E/da^2+2p/3]^{-1}, \tag{18}$$

where the cell parameter a is determined from Eq. (17) at $p=1$ atm. The differentiations in Eqs. (17) and (18) are *total* derivatives, carried out under conditions that the energy is minimized with respect to the shell model variables r and S.

The convergence conditions on r and S are that both $(\partial E/\partial r)/(\partial^2 E/\partial r^2)$ and $(\partial E/\partial S)/(\partial^2 E/\partial S^2)$ are $<1.\times10^{-7}$ nm. The convergence conditions on the parametrization are ±0.5 atm in the pressure, ±0.0001 kJ/mol in the energy and $\pm1\times10^{-8}$ atm^{-1} in the compressibility. The reliability of the assumptions used in estimating the long-range correction factor can be determined by the sensitivity of the intermolecular potential parameters to variation in the cutoff distance. Varying the cutoff from 1 to 2 nm has almost no influence on the parameters, $<0.7\%$ overall; the results are invariant for cutoffs greater than 1.5 nm. Thus our potential has been fully corrected for long range contributions to the energy. It is exact (for our model) and does not depend on a cutoff; put differently, the cutoff is ∞.

The site-site interaction potential Eq. (14) is a three parameter forms. Thermodynamic data on the α-phase can be accommodated by any of the six basic interaction site models. It can also be treated if we assume that *there are no shells* and that the intermolecular potential is simply the sum of potentials that are functions of the distance between atomic nuclei on different molecules or of the distance between molecular centers. In the latter case the molecular quadrupole is ignored (it cannot be modeled if the only interaction sites are the nuclei and the bond center) and there is no shell potential, and consequently no condensation induced shift of the N_2 stretching frequency.

All shell model interaction types exhibit the proper qualitative behavior, a red shift upon condensation to the solid phase; however, the numbers vary between 8 and 14 cm^{-1}, substantially smaller than the experimental value, 28 cm^{-1}. These shifts depend only on the extension of the atomic shells, which expand $\sim2.5\times10^{-4}$ nm during formation of the solid. The computed equilibrium bond length decreases by $<10^{-5}$ nm. It is possible that the inability of our shell model to better reproduce quantitatively the observed redshift reflects the fact that in parametrizing the basic molecular model we assumed both electrical and mechanical harmonicity of the shells, i.e. we ignored bond anharmonicity, hyperpolarizability (shell anharmonicity) and higher polarizability (field gradients); as noted, this limits the shell model's ability to account accurately for the influence of intense charge sources at small intermolecular separations. Changes in ν depend on third and higher derivatives of the potential, which are much less well determined than the potential function itself. Viewed from the perspective of the effect of condensation on nitrogen's vibrational frequency, the shell model represents an improvement over ''naked'' interaction site models. Choosing among the various ''dressed'' models requires consideration of other properties.

V. THE SECOND VIRIAL COEFFICIENT, $B(T)$

Computation of the second virial coefficient, $B(T)$, permits discrimination between interaction site models. This is an attractive alternative to performing many (hundreds or thousands) of *ab initio* calculations for various dimer geometries.[45] It is computationally much less intensive and, in accord with our general philosophy, uses experimental data to set the potential's parameters, thus being considerably more accurate. $B(T)$ is given by the expression[25]

$$B(T)=\frac{-N_{\text{Av}}}{4}\int_0^\infty R^2\,dR\int_0^\pi \sin\theta_1\,d\theta_1\int_0^\pi \sin\theta_2\,d\theta_2$$
$$\times\int_0^{2\pi} d\omega\,[e^{-u(R,\theta_1,\theta_2,\omega)/kT}-1], \tag{19}$$

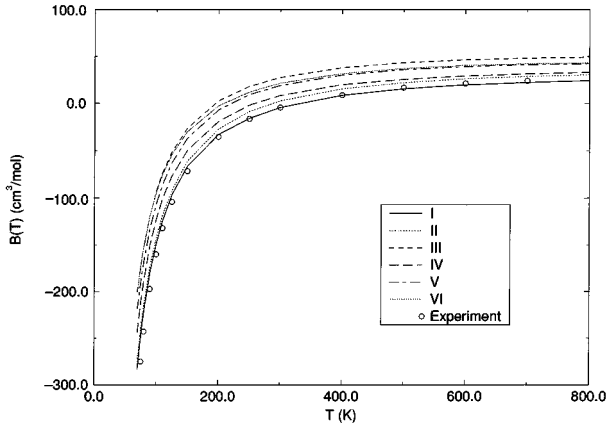

FIG. 4. Comparison of second virial coefficient, $B(T)$, as computed on the basis of various interaction site scenarios (see Table III and text) with experimental data over the accessible temperature range, $75<T<700$ K. Only type I and type II potentials are reasonable.

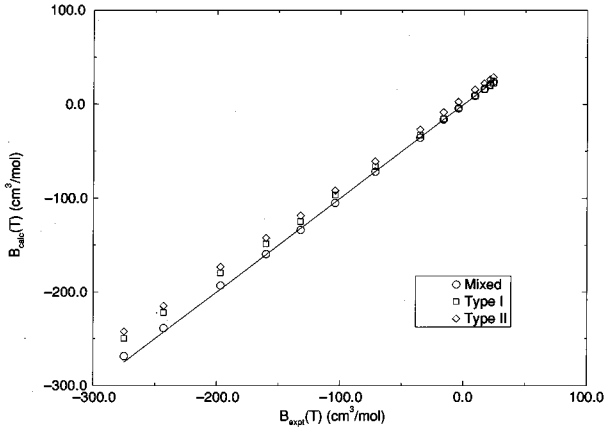

FIG. 5. Comparison of second virial coefficient, $B(T)$, as computed on the basis of type I, type II and mixed interaction site scenarios (see the text) with experimental data over the accessible temperature range, $75<T<700$ K; the experimental error bars are included. While type I and type II potentials are both reasonable, the mixed model reproduces the data precisely to within the experimental uncertainty.

where R is the distance between the molecular centers, θ_i the angle between the axis of molecule "i" and the intermolecular vector $\mathbf{R}$ and ω the dihedral angle between the planes $\mathbf{P}_1$ and $\mathbf{P}_2$ defined by the axes of molecule "i" and $\mathbf{R}$;[46,25] $u(R,\theta_1,\theta_2,\omega)$ is the pair potential and N_{Av} is the Avogadro number. Rigorous computation of $u(R,\theta_1,\theta_2,\omega)$ in the context of the shell model requires minimizing both shell locations and internuclear separations for each configuration. However, changes in bond length tend to be minimal. We computed $u(R,\theta_1,\theta_2,\omega)$ in an adiabatic approximation, with intramolecular N-N separation held fixed. Shell positions were adjusted to minimize the total dimer energy. The approximation was tested by comparing adiabatic and exact pair potentials for configurations in which the two N_2 molecules are parallel. The only noticeable differences arose for large interaction energies, equivalent to temperatures >2000 K, which contribute little in the experimental temperature range, $75<T<700$ K.[47,48] $B(T)$ was computed using a four-dimensional Gauss-Legendre integral quadrature. The total energy was minimized with respect to the 18 shell variables using a conjugate gradient minimizer. The integration was broken into two regions, <0.5 nm and 0.5–1.5 nm and a long range correction formula (Appendix B) developed for $R>1.5$ nm. At higher temperatures the full procedure, minimization of u for a particular intermolecular configuration, and integration until convergence, required up to 3 minutes CPU time on a Silicon Graphics Indigo R4400.

Comparisons of $B(T)$ computed on the basis of different interaction site models are summarized in Figure 4. Only two of the possibilities tested provide good first approximations: interactions between the bond shells of the two molecules (type I) or between the atomic shells of one molecule and the bond shell of the other (type II). Either yields results close to the experimental values over the whole temperature range, 75–700 K, although there are some small discrepancies. For interaction of type II, $B(T)$ is always slightly too large. For type I interaction, there is a crossover; at low T, $B(T)$ is too large and at high T, too small. Other interaction schemes, including those ignoring the shells (not illustrated), lead to uniformly high predictions. This is very encouraging. The shell model posits that the "non-classical" terms in the interaction potential should involve coupling between shells. Of the various schemes devised to account for the solid phase data, those that presumed the intermolecular contribution to couple the nuclei, either with one another or with the shells, failed.

We then developed a six parameter form, mixing type I and type II coupling, to more accurately reproduce the virial data. The results are summarized in Table IV and Figure 5. The Table contrasts the parameter sets for the type I, type II and mixed models. Although the parameters seem quite different, the potentials are not dissimilar as the value of W_{LR}, the coefficient of the long range R^{-6} term, makes evident. Type I and type II potentials differ by $<9\%$ and the difference between either type I or type II potentials and the "mixed" model is $<6\%$. The Figure contrasts experiment

TABLE IV. Parameters for Type I, II and "mixed" models.[a]

Interaction type	ϵ_{I}/K	σ_{I}/nm	α_{I}	ϵ_{II}/K	σ_{II}/nm	α_{II}	W_{LR}/Knm^6
I	99.30	0.4201	11.533	⋯	⋯	⋯	−1.138
II	⋯	⋯	⋯	35.13	0.3833	10.485	−1.042
Mixed	32.76	0.4531	11.51	32.00	0.3457	10.46	−1.105

[a]W_{LR} is the coefficient of the long range, continuum, R^{-6} contribution to the pair interaction energy (see Appendix B).

with the computed values of $B(T)$. The 6 parameter model replicates the data perfectly. We might expect that the potential should also include some type III interaction, between the atomic shells on different molecules. However, as is evident from Figure 4, pure type III coupling cannot reproduce $B(T)$. Efforts to incorporate such a term, by assuming that there should be combining rules relating the parameters of type I, II and III potentials (constrained to 6 independent parameters), were uniformly unsuccessful.

VI. APPLICATIONS

Of the three possible intermolecular potentials for nitrogen, the ''mixed'' model reproduces $B(T)$ perfectly; however, it has the drawback of having been slightly adjusted to fit the data. Is there any reason to believe that the mixed model is superior to either models I or II?

To address this question consider another low temperature phase of nitrogen, the tetragonal γ-phase, stable at low temperature and at pressures between 3.6 and 20 kbar.[36,49,50] There are two molecules per unit cell. The corner one is oriented along the face diagonal; the body molecule is oriented perpendicular, but in the parallel plane. The symmetry is such that N_2 remains a linear quadrupole. At 20.5 K and 4015 atm the unit cell parameters are $a=0.3957$ nm, $c=0.5109$ nm, corresponding to a c/a ratio of 1.291.[49,50] The total crystal energy is of the form of Eq. (15) but the coordination shells reflect changed symmetry. Instead of being concentric spheres, they are now concentric ellipsoids of revolution. There are two sets of molecular indices (i,j,k): the body sites $[2l+1,2m+1,2n+1]$ and the corner sites $[2l,2m,2n]$. The Nth coordination shell is defined slightly differently: there are two components, corner molecules for which $N=(l^2+m^2+n^2)$ or body molecules for which $N=(l^2+m^2+n^2)+(l+m+n)+1$. The energy is decomposed into three contributions, an intramolecular shell relaxation term, an exact summation reflecting the interaction of a central molecule with the first N_c coordination shells, and a long range term describing the coupling to more distant molecules (see Appendix B). The thermodynamic properties can be computed as before. For given a and c, shells and bonds relax to minimize the energy; the c/a ratio is adjusted to minimize the energy and the pressure is determined from the thermodynamic constraint, Eq. (17). The result is

$$p=-\frac{2}{3a^2c}\left[a\,\frac{\partial E}{\partial a}+c\,\frac{\partial E}{\partial c}\right] \tag{20}$$

$$0=\left[a\,\frac{\partial E}{\partial a}-2c\,\frac{\partial E}{\partial c}\right]. \tag{21}$$

Table V compares the consequences of the 3 different interaction schemes with experiment. Before discussing the results, it must be emphasized that the long range terms have been carefully analyzed and accurately accounted for (see Appendix B). Our conclusions are unaltered if we treat anywhere from 7 to 25 coordinate shells exactly. This is important because the effects that are being studied, the differences between the thermodynamic properties of the two phases, are extremely small. The most striking conclusion is that neither type I nor type II interaction schemes predicts a phase transition, while the ''mixed'' potential, the one which exactly reproduced $B(T)$, does. For interaction of type I, the α-phase is predicted to be the stable form at all pressures. Both $H_\alpha<H_\gamma$ and $v_\alpha<v_\gamma$; compressing the system only accentuates the stability of the α-phase. For type II interaction, the γ-phase is always more stable; both inequalities are reversed. However, for the ''mixed'' model, a new feature emerges. At $p=0$, the α-phase is more stable, $H_\alpha<H_\gamma$. However, the γ-phase has the smaller molar volume, $v_\alpha>v_\gamma$; increasing the pressure favors the γ-phase. There is a phase transition at $\sim$10 kbar. While the transition pressure is about three times that which is observed, the only other nitrogen intermolecular potential that reproduces this phase transition was specially parametrized to fit the *P-V* curve of the α-phase.[51] To our knowledge, potentials applicable over a wide *PVT* domain have not successfully simulated this transition. In analyzing the phase transition, the importance of properly treating the long range contributions to the enthalpy cannot be emphasized too strongly; the computed and estimated experimental transition enthalpies are small and comparable to the size of the long range contributions at the shorter cutoff. In addition to the natural appearance of a phase transition, the calculations using the ''mixed'' potential provide reasonable estimates of the heat and volume of transition at $p=1$ atm, although these numbers can only be roughly estimated. Our computed value of the anisotropy ratio c/a is 4% too high; the calculated values for a and c are good, 1.3% too small and 2.7% too large respectively.

TABLE V. Some properties of the γ-phase at $p=1$ bar.

Interaction type	$\Delta H_{\alpha\to\gamma}$ (kJ/mol)	$\Delta v_{\alpha\to\gamma}$ (cm^3/mol)	c/a
I	+0.235	+0.323	1.360
II	−0.158	−0.611	1.339
Mixed	+0.103	−0.066	1.345
Experiment	+0.059[a]	−0.165[b]	1.291[c]

[a]Computed from Δv at triple point (Ref. 11) and transition pressure at 0 K.
[b]Reference 66.
[c]References 36, 49, and 50.

Using the ''mixed'' potential we simulated the liquid at a density and temperature corresponding to its normal (1 atm) boiling point, 0.8081 g/cm^3 and 77.35 K. Two 20 ps simulations were performed with a modified version of the GROMACS[52] molecular dynamics simulation package. The simulation parameters are summarized in Table VI. Both were carried out at constant volume and temperature was controlled using the Berendsen coupling method.[53] As in the case of the solid phases, the shell variables had to be tightly minimized at each MD step. Our measure is the quantity Δx, defined as

$$\Delta x=\sqrt{\frac{1}{3N}\sum_i^{3N}\left(\frac{f_i}{k_i}\right)^2}, \tag{22}$$

where f_i is the force on a shell and $k_i=1/\alpha_i$ the corresponding force constant; there are $3N$ terms in the sum since each molecule contains three shells. Here f_i is the norm of the force acting on the ith shell. The average displacement of the

TABLE VI. Parameters of the liquid simulation.

Number of molecules	216
Cube length	2.3163 nm
Time of equilibration	8[a] or 10[b] ps
Time of data collection	20 ps
Time step	0.5 fs
Cutoff radius	0.9 nm
SHAKE tolerance	1.0×10^{-8} nm
Shell tolerance (Δx)	1.0×10^{-7} nm
Temperature coupling constant	0.05[a] or 0.5[b] ps

[a]Simulation I.
[b]Simulation II.

shells from the position of zero force is thus smaller than Δx. Just as in the case of the solid phases the tolerance is small, 1.0×10^{-7} nm. Simulations I and II differed only in the value of the temperature coupling constant, 0.05 ps and 0.5 ps respectively.

Since a 0.9 nm cutoff was used, long range corrections to the energy and the pressure are significant. The expressions are given in Appendix B. The results of our simulations are summarized in Figure 6 and Table VII. The statistical uncertainties quoted are estimated by the sub-average method.[46] Figure 6 compares our pair correlation function with experiment;[54] there are slight differences in the peak heights and the slope of the first peak, and the experimental $g(r)$ exhibits some additional structure near the first peak and first minimum. While theory and experiment are essentially superposable to within the experimental uncertainty, it is most likely that the first peak should exhibit some asymmetry due to molecular size effect,[14,54] suggesting a possible limitation of our potential, some of which may reflect the neglect of quantum corrections.[55] In particular, we would expect $g(r)$ to be somewhat smaller at the maxima. There is little difference between $g(r)$ in the two simulations. Simulated and experimental $g(r)$'s are in phase, suggesting that the repulsive interactions have been realistically modeled.[54] We have estimated the occupancy of the first and second coordination shells by integrating the area under the first and second coordination peaks; differences between simulation and experiment are small. The mean pressures in the two runs are 0.124 and 0.056 kbar respectively. The enthalpy of vaporization is computed as

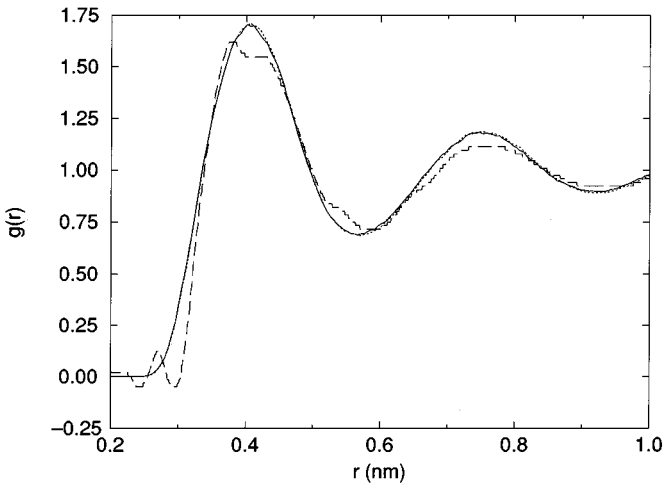

FIG. 6. Comparison of N-N (atom-atom) radial distribution function as computed in simulations I (dotted line) and II (dashed line) with experiment (solid line) (Ref. 54). The experimental structure between 0.25 and 0.3 nm is an artifact. That observed near the first peak (0.4 nm) and the first minimum (0.55 nm) is not reproduced by our simulations and may reflect deficiencies of our model potential function and the neglect of quantum corrections (Ref. 55).

TABLE VII. Summary of liquid simulations.

	I	II	Experiment
ρ (g/cm^3)	0.808123	0.808123	0.8081
T (K)	77.26±0.06	76.94±0.20	77.35
$\bar{p}$ (kbar)	0.124±0.013	0.056±0.010	0.001
D[a] (cm^2/s)	2.85×10^{-5}	2.35×10^{-5}	2.6×10^{-5} [b]
D[c] (cm^2/s)	2.71×10^{-5}	2.22×10^{-5}	2.6×10^{-5} [b]
ΔH_{vap} (kJ/mol)	−6.033	−6.155	−5.569[d]
ϵ	1.453	1.453	1.433[d]
Occupancy, 1st shell	6.5	6.5	6.75
Occupancy, 2nd shell	21.8	21.8	22.0

[a]D from mean square displacement.
[b]Reference 67.
[c]D from velocity autocorrelation function.
[d]Reference 58.

$$\Delta H_{vap} = U(\text{liq}) + pV(\text{liq}) - U(\text{gas}) - pV(\text{gas})$$
$$= E_{pot}(\text{liq}) + pV(\text{liq}) - E_{pot}(\text{gas}) - nRT \qquad (23)$$

where nitrogen vapor is presumed to behave as an ideal gas. Two quantum corrections have been included. The first accounts for the vibrational shift between the gas phase ω_e and the experimental liquid phase frequency, -30.9 cm^{-1};[56] it contributes $+0.185$ kJ/mol to ΔH_{vap}. The second treats the low frequency phonon spectrum of the liquid, which, extrapolated from measurements at 122 K and 87.3 K,[57] we estimate to peak at ~ 63 cm^{-1} at the boiling point, 77.35 K; this contributes -0.073 kJ/mol to ΔH_{vap}. In addition, the liquid state energies have been extrapolated to 1 bar; since $(\partial U/\partial p)_T = V(p\kappa_T - T\alpha_p)$, using the experimental values of κ_T and α_p[58] the extrapolation contributes -0.179 and -0.082 kJ/mol to simulations I and II respectively. Thus corrected, the two ΔH_{vap} values differ < 0.6 kJ/mol from experiment. The long range contribution is again significant, -0.339 kJ/mol, $\sim 6\%$ of the total heat of transition.

To show that our potential function describes more than just bulk thermodynamic properties, we computed the self-diffusion coefficient (a measure of spatial correlation) and the dielectric constant (a measure of angular correlation). The molecular diffusion coefficient, D, was computed from the slope of the average mean square displacement of the molecular center; the statistical uncertainty in this result has been estimated as $\sim \pm 17\%$.[59] An alternate estimate of D is found from the velocity autocorrelation function; the two sets of results are in good agreement. The dielectric constant is computed by averaging the form of the statistical mechanical Clausius-Mossotti equation applicable to non-polar molecules[60,61]

TABLE VIII. Low energy conformations of the N_2 dimer.

	Ab initio[a]		Shell model	
Conformation	ΔE_{stab}/kJ mol^{-1}	R/nm	ΔE_{stab}/kJ mol^{-1}	R/nm
"cross"	−1.5	0.36	−0.8	0.41
"parallel"	−1.3	0.37	−0.6	0.42
"tee"	−1.0	0.41	−1.1	0.43
"linear"	−0.2	0.52	−0.1	0.47

[a]Reference 28.

$$\frac{\epsilon-1}{\epsilon+2}=\frac{4\pi\rho\alpha}{3}+\frac{4\pi\rho}{9NkT}[\langle\mathbf{M}^2\rangle-\langle\mathbf{M}\rangle^2], \tag{24}$$

where $\mathbf{M}$ is the total dipole moment at each step of the simulation and N the number of molecules in the simulation. In non-polar fluids such as liquid nitrogen, the polarizability provides the major contribution to the dielectric ratio $(\epsilon-1)/(\epsilon+2)$ and the fluctuation term ($\sim$3.5% of the total) is only a small correction. The computed values of both D and ϵ are in excellent accord with experiment. Our potential function is reliable over a wide range of temperature and density, and accounts for correlation phenomena.

VII. COMPARISON WITH *AB INITIO* RESULTS

Van der Avoird[28,62] has carried out extensive *ab initio* studies of N_2, developing an intermolecular potential and using it to compute the virial coefficient and properties of the low temperature solid phases. Our potential differs from theirs in a number of respects. The data are contrasted in Table VIII. Quantum calculations indicate that the lowest energy state of the dimer is the "cross" conformation, followed by "parallel," "tee" and "linear";[28] our potential exhibits different ordering, stabilization energies and intermolecular separations. Except for the "tee" the energies and intermolecular separations are quite different. Our stabilization energies are half as large and the R values are not as variable. However, the *ab initio* potential, when used to compute thermodynamic properties, requires significant scaling of the repulsive overlap terms to fit the virial data or to account for thermodynamic properties of the α phase.[62] This modified *ab initio* potential is phase transferable. It accounts for $B(T)$, the phonon frequencies of both α and γ phases and the energy, density and compressibility of the α phase. It correctly identifies the α phase as the low pressure phase, but it does not predict the phase transition, even if the lattice parameters of the γ phase are fit to experimental data at p=1 atm; $\Delta H_{\alpha\rightarrow\gamma}$ is far too large. Being a numerical potential, it did not lend itself to liquid state simulations.

Can any conclusions be drawn from these considerations? Most immediately, we see that *ab initio* quantum studies, even done with immense refinement, still do not adequately describe interacting nitrogen molecules. Only after an empirical modification do they reproduce thermodynamic behavior. Little can then be concluded about the differences between our empirical potential function and either the unmodified or the modified quantum results. Possibly the most reasonable observation is the one we presented as a rationale for our kind of modeling: a more reliable potential can often be found by fitting to experimental data than by *ab initio* computations.

VIII. SUMMARY AND FUTURE PROSPECTS

We have presented a generalizable approach to the development of phase transferable effective intermolecular potentials and applied the method to the study of N_2. The method is based upon construction of a shell model description of the isolated molecule using experimental data to establish the parameters. Modeling the Ne dimer demonstrates that this is a conceptual advance over point polarizability treatments. When applied to N_2 we obtain a parametrization that accurately describes not only the electrostatic field surrounding the molecule (i.e. a practical representation of the molecular charge distribution) but also the isolated molecule's response to electrical and mechanical stress (polarization and deformation). Nitrogen is described by means of five charge centers: the nuclei, two atomic shells and a bond shell. The shells are bound to their respective nuclei by means of polarization springs. As the molecular model accurately accounts for both polarization and electrostatics, the purely intermolecular part of our potential function is not biased by errors in our treatment of the molecule. We find that the intermolecular terms should be based upon shell-shell interactions, consistent with our identification of the shells as representations of the molecular charge distribution. These intermolecular terms are parametrized by fitting properties of the low temperature solid phase of nitrogen. A particular interaction scheme, coupling the bond shells with one another and with the other molecule's atomic shells yields a phase transferable potential able to account for the second virial coefficient of the gas phase, the pressure induced phase transition between nitrogen's cubic and tetragonal phases, and a wide range of liquid properties (pair distribution function, heat of vaporization, self-diffusion coefficient and dielectric constant).

Our potential is based on a molecular description with separable atomic and bond contributions. The purely intermolecular terms involve interaction between shells on different molecules. We plan to apply the same general approach to constructing effective potentials for O_2 and NO, first to see how our decompositional scheme can be applied to other molecules and then to determine if the atomic shell behavior of N in N_2 and O in O_2 are transferable to the treatment of NO. The same general procedure can be applied to the development of potential functions for H_2O and HF. This provides a critical test of the method, since the treatment of dipolar molecules requires substantial elaboration of the basic approach. Finally, it is clear that our method for describing the molecular charge distribution naturally decomposes into atomic and bond contributions. This suggests that larger molecules (such as hydrocarbons) should be easily described by an extension of the method, constructing the potential function for the molecule by means of transferable components.

ACKNOWLEDGMENTS

All quantum chemical calculations were performed on the CONVEX 3860 at the Slovenian Supercomputer Center using the GAUSSIAN-90 suite of programs. One of us (J.M.) thanks the Human Frontier Science Program for a long term fellowship. The work was carried out during a sabbatical leave from Brandeis University and was supported by Grant No. GM-28643 from the National Institutes of Health (P.C.J.). J.M. and P.C.J. are grateful to the University of Groningen and the Molecular Dynamics group for hospitality during their stays in the Netherlands. We wish to thank Dr. David Woon for calculating the Ne_2 quadrupole moments and Dr. C.G. Gray and Dr. P. Egelstaff for helpful comments.

APPENDIX A: SHELL MODEL EQUATIONS

Equations (9)–(13) define the shell potential and establish the basic set of shell parameters consistent with the molecular data set $\alpha_\parallel, \alpha_\perp, R_o, k_{\rm vib}, M_4$ and M_{16}. The shell potential energy, Eq. (9), is minimized with respect to the shell displacements. At equilibrium, in the absence of an external field, the charges are collinear; the bond shell is not displaced and the atomic shells are displaced a distance z exterior to the nuclei. Minimization with respect to z yields

$$z/\alpha_a+(1+\sigma)(f-Df')/D^2+2\sigma(d^{-2}-w')+\Delta^{-2}-v'=0, \tag{A1}$$

where we have divided by q_a^2 and suppressed the identifying subscripts on $f_{\rm shld}, w_{a-b}$ and v_{b-b}; the arguments of the three functions are $D=R-z, d=R/2-z$ and $\Delta=R-2z=2d$ respectively and $\sigma\equiv q_b/(2q_a)$. R is always evaluated at the equilibrium bond length, R_o and z at the equilibrium shell displacement, $z_{\rm eq}$. Minimizing with respect to R yields

$$2\sigma^2R/\alpha_b-(1+\sigma)^2/R^2+2(1+\sigma)(f-Df')/D^2-2\sigma(d^{-2}-w')-\Delta^{-2}+v'=0. \tag{A2}$$

Analogous to the expression for M_4, Eq. (8), that for the hexadecapole moment is

$$M_{16}=q_bS^4-q_az(R+z)(R^2+2Rz+2z^2). \tag{A3}$$

The expressions determining $\alpha_\parallel$ and $\alpha_\perp$ are complex. With the field perpendicular to the molecular axis, $E_\perp$, the atomic shells are displaced an equal amount, x, while the bond shell is displaced by x_o. Minimizing the energy, subtracting out the constraint determining $z_{\rm eq}$, Eq. (A1), we obtain the simultaneous equations

$$(a_\perp-b_\perp)x+b_\perp x_o=E_\perp/q_a$$

$$b_\perp x+(c-b_\perp)x_o=\sigma E_\perp/q_a$$

where

$$a_\perp=\alpha_a^{-1}+(1+\sigma)(f-Df')/D^3$$

$$b_\perp=2\sigma(d^{-2}-w')/d$$

$$c=4\sigma^2/\alpha_b.$$

Since

$$\alpha_\perp=(2q_ax+q_bx_o)/E_\perp,$$

we find that

$$\alpha_\perp=\frac{2[\sigma^2a_\perp-(1+\sigma)^2b_\perp+c]}{a_\perp c-b_\perp(a_\perp+c)}. \tag{A4}$$

With the field parallel to the molecular axis, $E_\parallel$, the atomic shells are displaced an equal amount, y, while the bond shell is displaced by y_o. Shell 1 is now at $-z+y$ and shell 2 at $z+y$. After minimizing the energy and subtracting Eq. (A1), the result is

$$(a_\parallel+b_\parallel)y-b_\parallel y_o=E_\parallel/q_a$$

$$-b_\parallel y+(c+b_\parallel)y_o=\sigma E_\parallel/q_a$$

where

$$a_\parallel=\alpha_a^{-1}-2(1+\sigma)(f-Df'+D^2f''/2)/D^3$$

$$b_\parallel=2\sigma(2/d^3+w'')$$

$$c=4\sigma^2/\alpha_b.$$

Since

$$\alpha_\parallel=(2q_ay+q_by_o)/E_\parallel,$$

we find that

$$\alpha_\parallel=\frac{2[\sigma^2a_\parallel+(1+\sigma)^2b_\parallel+c]}{a_\parallel c+b_\parallel(a_\parallel+c)}. \tag{A5}$$

The final constraint is that determining $k_{\rm vib}$; this requires computing $d^2U_{\rm shell}/dR^2$ subject to the condition that the potential energy function is always minimized with respect to the shell displacements. The result is

$$k_{\rm vib}=d^2U/dR^2=\partial^2U/\partial R^2-(\partial^2U/\partial R\partial z)^2/(\partial^2U/\partial z^2), \tag{A6}$$

where

$$\partial^2U/\partial R^2=q_a^2[2\sigma^2/\alpha_b+2(1+\sigma)^2/R^3-4(1+\sigma)(f-Df'+D^2f''/2)/D^3+\sigma(2/d^3+w'')+2\Delta^{-3}+v'']$$

$$\partial^2U/\partial R\partial z=q_a^2[8(1+\sigma)(f-Df'+D^2f''/2)/D^3-2\sigma(2/d^3+w'')-2\Delta^{-3}-v'']$$

$$\partial^2U/\partial z^2=q_a^2[2/\alpha_a-8(1+\sigma)(f-Df'+d^2f''/2)/D^3+4\sigma(2/d^3+w'')+8\Delta^{-3}+4v''].$$

The seven defining equations [(8) and (A1)–(A6)] have been displayed in their full generality. However, as indicated in Section III, we presume both that $f_{\rm shld}\equiv1$ and that $v_{a-a}\equiv0$ and thus that all their derivatives are zero. Limiting ourselves to determination of w' and w'' in the stable configuration, where $d=R_o/2+z_{\rm eq}$, establishes the shell parameters.

APPENDIX B: LONG RANGE CORRECTIONS

Treatment of the long range contributions to the energy is critical for all calculations: parameter determination and thermodynamics. The potentials all contain three fundamental intermolecular terms: short range core, long range electrostatic, and long range dispersion. At the cutoff distances we will be using, >1 nm, the core terms are insignificant. This is not true of the electrostatic and dispersion contribu-

tions. However, at large intermolecular separations the molecule can be treated as a single force center with all intermolecular contributions translated to the molecular origin (the midpoint of the bond). The validity of the assumption can be tested by seeing if results are sensitive to variation of the cutoff distance.

The interaction energy between a pair of molecules separated by more than R_c, the cutoff distance, has the form[25]

$$u_{\mathrm{LR}}=0.75Q^2F(\theta_1,\theta_2,\omega)/R^5+W_{LR}/R^6 \tag{B1}$$

$$\begin{aligned}F(\theta_1,\theta_2,\omega)=&1-5\sin^2\theta_1-5\sin^2\theta_2+17\sin^2\theta_1\sin^2\theta_2\\&+2\cos^2\theta_1\cos^2\theta_2\cos^2\omega\\&-16\sin\theta_1\sin\theta_2\cos\theta_1\cos\theta_2\cos\omega\end{aligned} \tag{B2}$$

with θ_1,θ_2 and ω defined as discussed in Section V. Q is the quadrupole moment, which, due to shell interaction, is slightly different in condensed phases than in the gas phase and F is the angular factor for the interaction of a pair of quadrupoles; W_{LR} is the dispersion contribution to the intermolecular shell potential. For Buckingham type potentials, Eq. (14), this has the form

$$W_{\mathrm{LR}}=-f_{\mathrm{type}}\epsilon\sigma^6/(1-6/\alpha); \tag{B3}$$

the multiplicity factor f_{type} accounts for the number of interaction site pairs for the potential of interest. It equals 4 except for type I and type V interactions (see Table III), where it is 1 and 8 respectively. The long range correction must be computed separately for each phase.

At sufficiently large intermolecular separations the exponential in Eq. (19) can be expanded in Taylor series and the first two terms kept; the correction to the virial coefficient, $B_{\mathrm{LR}}(T)$, is simply

$$\begin{aligned}B_{\mathrm{LR}}(T)=&\frac{N_{\mathrm{Av}}}{4kT}\int_{Rc}^{\infty}R^2\,dR\int_0^{\pi}\sin\theta_1\,d\theta_1\int_0^{\pi}\sin\theta_2\,d\theta_2\\&\times\int_0^{2\pi}d\omega\;u_{LR}(R,\theta_1,\theta_2,\omega).\end{aligned} \tag{B4}$$

The result is

$$B_{\mathrm{LR}}(T)=\frac{\pi N_{\mathrm{Av}}}{kT}[3Q^2/2R_c^2+2W_{\mathrm{LR}}/3R_c^3]. \tag{B5}$$

In the solid phases the molecules' relative orientation is not random and simple angle averaging is incorrect. If the cutoff is large enough so that the pair correlation function in the solid, $g(\mathbf{r}_1,\mathbf{r}_2)$, approaches its long range value of 1, the continuum approximation to Eq. (15) is

$$U_{\mathrm{LR}}(R_c)=0.5\int_{Rc}^{\infty}R^2\,dR\int_0^{\pi}\sin\chi\,d\chi\int_0^{2\pi}d\phi\;\rho\;u_{\mathrm{LR}}(R,\chi,\phi) \tag{B6}$$

where ρ is the number density and u_{LR} the long range contribution to the energy, given by Eqs. (B1) and (B2). Both the cutoff distance and the number density are related to the cell constant a, $\rho=4/a^3$ and $R_c=a\sqrt{(N_c/2)}$. Specifically exhibiting the dependence on the cell constant is imperative in order to properly treat the volume dependence. This procedure is identical to the volume scaling used to determine the virial in statistical mechanics.[63] Integration of the R^{-6} term is trivial; handling the quadrupolar term is more difficult because each χ and ϕ defined by the structural sublattices of the α-phase determine specific values of θ_1,θ_2 and ω. Corner and face sites of the fcc lattice must be treated separately. At the corners we find that $\theta_1=\pi/2-\chi,\theta_2=\pi/2-\chi$ and $\omega=0$, and the factor F_{corner} of Eq. (B2) reduces to

$$F_{\mathrm{corner}}=3-30\cos^2\chi+35\cos^4\chi \tag{B7}$$

which averages to 0. Analysis of the three face sublattices is more cumbersome; quadrupolar interaction again contributes nothing to the long range correction. A typical factor is

$$\begin{aligned}F_{\mathrm{face}}=&1-5\cos^2\chi-(5-17\cos^2\chi)(\cos^2\chi+2\\&\times\sin^2\chi\cos^2\omega)/3+2\sin^2\chi(\sin^2\chi+2\\&\times\cos^2\chi\cos^2\omega)/3-16\sin^2\chi\cos^2\chi(1-2\cos^2\omega)/3.\end{aligned} \tag{B8}$$

The long-range correction for the cubic α-phase is

$$U_{\mathrm{LR}}=\frac{8\pi W_{\mathrm{LR}}}{3a^3R_c^3},\quad R_c=a\sqrt{(N_c/2)}. \tag{B9}$$

For the tetragonal phase the analog to Eq. (A12) is

$$U_{\mathrm{LR}}(R_c)=0.5\int_{cN}^{\infty}dz\int_{r(z)}^{\infty}r\,dr\int_0^{2\pi}d\phi\;\rho\;u_{\mathrm{LR}}(z,r,\phi) \tag{B10}$$

where the density is now $\rho=2/(a^2c)$ and the ellipsoidal cutoff envelope is defined by $r(z)=\sqrt{[N^2a^2-z^2a^2/c^2]}$. Transforming to spherical coordinates this becomes

$$\begin{aligned}U_{\mathrm{LR}}(R_c)=&0.5\int_0^{\pi}\sin\chi\,d\chi\int_{R(\chi)}^{\infty}R^2\\&\times dR\int_0^{2\pi}d\phi\;\rho\;u_{\mathrm{LR}}(R,\chi,\phi)\end{aligned} \tag{B11}$$

where $R(\chi)=Nac/\sqrt{[a^2\cos^2\chi+c^2\sin^2\chi]}$ and Eqs. (B1) and (B2) determine u_{LR}. The arguments of F, Eq. (B2), again depend on χ and ϕ. For the body and corner sites we find the following expressions:

$$\begin{aligned}F_{\mathrm{body}}=&8-24\sin^2\chi+19\sin^4\chi-16\sin^2\chi\cos^2\chi\\F_{\mathrm{corner}}=&-4+5\sin^2\chi+12\sin^2\chi\sin^2\phi-17\sin^4\chi\sin^2\phi\\&+18\sin^2\chi\cos^2\chi\sin^2\phi.\end{aligned}$$

The quadrupolar terms average to zero (R integration precedes χ integration) with the result

$$U_{\mathrm{LR}}=\frac{\pi W_{\mathrm{LR}}}{2N_c^3}\left[\frac{1}{a^4c^2}+\frac{2}{3a^2c^4}+\frac{\sin^{-1}\omega}{a^5c\omega}\right],\quad \omega=\sqrt{(1-a^2/c^2)}. \tag{B12}$$

In the liquid phase the long range corrections to the energy and pressure can be estimated if we assume the cutoff is large enough so that $g(\mathbf{r}_1,\mathbf{r}_2)$ can be approximated by its long range value of 1. While it is clear from the data of Figure 6 that this condition is not completely satisfied at the 0.9 nm cutoff, most of the structure in g($\mathbf{r}_1$, $\mathbf{r}_2$) has been damped out. The energy correction can be determined by

combining the arguments leading to Eqs. (B6) and (B4); the resulting correction to the energy per particle is

$$U_{\mathrm{LR}}(R_c)=2\pi\rho[3Q^2/4R_c^2+W_{\mathrm{LR}}/3R_c^3]. \tag{B13}$$

Similarly, the long range correction to the pressure can be evaluated from standard expressions;[64] the result is

$$p_{\mathrm{LR}}(R_c)=\pi\rho^2[5Q^2/2R_c^2+4W_{\mathrm{LR}}/3R_c^3]. \tag{B14}$$

[1] There is an enormous literature on the development of effective intermolecular potentials. For a review which deals extensively with the most studied example, water, see S.-B. Zhu, S. Singh, and G.W. Robinson, Adv. Chem. Phys. **85**, 733 (1993).
[2] H.J.C. Berendsen, J.P.M. Postma, W.F. van Gunsteren, and J. Hermans, in *Intermolecular Forces*, edited by B. Pullman (Reidel, Dordrecht, The Netherlands, 1981).
[3] W.L. Jorgensen, J. Chandrasekhar, J.D. Madura, R.W. Impey, and M.L. Klein, J. Chem. Phys. **79**, 926 (1983).
[4] For the most ambitious recent study of this sort, see J.R. Maple, M.-J. Hwang, T.P. Stockfisch, U. Dinur, M. Waldman, C.S. Ewig, and A.T. Hagler, J. Comput. Chem. **15**, 162 (1994).
[5] J.W. Halley, J.R. Rustad, and A. Rahman, J. Chem. Phys. **98**, 4110 (1993).
[6] U. Niesar, G. Corongiu, E. Clementi, G.R. Kneller, and D.K. Battacharya, J. Phys. Chem. **94**, 7949 (1990).
[7] S.-B. Zhu, S. Singh, and G.W. Robinson, J. Chem. Phys. **95**, 2791 (1991).
[8] R. Car and M. Parrinello, Phys. Rev. Lett. **55**, 2471 (1985).
[9] K. Laasonen, M. Sprik, and M. Parrinello, J. Chem. Phys. **99**, 9080 (1993).
[10] B.G. Dick, Jr. and A.W. Overhauser, Phys. Rev. **112**, 90 (1958).
[11] L.R. Pratt, Mol. Phys. **40**, 347 (1980).
[12] J.S. Hǿye and G. Stell, J. Chem. Phys. **73**, 461 (1980).
[13] M. Sprik and M.L. Klein, J. Chem. Phys. **89**, 7556 (1988).
[14] C.G. Gray and K.E. Gubbins, *Theory of Molecular Fluids* (Oxford University Press, New York, 1984).
[15] C.-H. Kiang and W.A. Goddard III, J. Chem. Phys. **98**, 1451 (1993).
[16] C.A. Coulson, *Valence* (Oxford University Press, New York, 1952).
[17] R. Eggenberger, S. Gerber, H. Huber, and D. Searles, Chem. Phys. **156**, 395 (1991).
[18] D.E. Woon, J. Chem. Phys. **100**, 2838 (1994).
[19] S.F. Boys and F. Bernardi, Mol. Phys. **19**, 553 (1970).
[20] D.E. Woon (private communication).
[21] M. J. Frisch *et al.*, *Gaussian 90, Revision H* (Gaussian, Inc., Pittsburgh PA, 1990).
[22] G. Herzberg, *Spectra of Diatomic Molecules* (van Nostrand, New York, 1950).
[23] J.D. Poll and J.L Hunt, Can. J. Phys. **59**, 1448 (1981).
[24] E.R. Cohen and G. Birnbaum, J. Chem. Phys. **66**, 2443 (1977).
[25] J.O. Hirschfelder, C.F. Curtiss, and R.B. Bird, *Molecular Theory of Gases and Liquids* (Wiley, New York, 1954).
[26] T.B. MacRury, W.A. Steele, and B.J. Berne, J. Chem. Phys. **64**, 1288 (1976).
[27] J.C. Raich and N.S. Gillis, J. Chem. Phys. **66**, 846 (1977).
[28] R.M. Berns and A. van der Avoird, J. Chem. Phys. **72**, 6107 (1980).
[29] J.E. Gready, G.B. Bacskay and N.S. Hush, Chem. Phys. **31**, 467 (1978).
[30] R.D. Amos, Mol. Phys. **39**, 1 (1980).
[31] F. Mulder, G. van Dijk, and A. van der Avoird, Mol. Phys. **39**, 407 (1980).
[32] M. Moon and D.W. Oxtoby, J. Chem. Phys. **84**, 3830 (1986).
[33] H.-J. Werner and W. Meyer, Phys. Rev. A **13**, 13 (1976).
[34] T.M. Miller and B. Bederson, Adv. At. Mol. Phys. **13**, 1 (1977).
[35] A.J. Stone and S.L. Price, J. Phys. Chem. **92**, 3325 (1988).
[36] T.A. Scott, Phys. Rep. **27**, 89 (1976).
[37] F. Medina and W.B. Daniels, Phys. Rev. Lett. **32**, 167 (1974).
[38] M. Thiery and V. Chandrasekharan, J. Chem. Phys. **67**, 3659 (1977).
[39] D.C. Heberlein, E.D. Adams, and T.A. Scott, J. Low Temp. Phys. **2**, 449 (1970).
[40] B.C. Kohin, J. Chem. Phys. **33**, 882 (1960).
[41] W.F. Giauque and J.O. Clayton, J. Am. Chem. Soc. **55**, 4875 (1933).
[42] J.K Kjems and G. Dolling, Phys. Rev. B **11**, 1639 (1975).
[43] R. LeSar and R.G. Gordon, J.Chem. Phys. **78**, 4991 (1983).
[44] R.D. Etters, V. Chandrasekharan, E. Uzan, and K. Kobashi, Phys. Rev. B **33**, 8615 (1986).
[45] O. Matsuoka, E. Clementi, and M. Yoshimine, J. Chem. Phys. **64**, 1351 (1976).
[46] M.P. Allen and D.J. Tildesley, *Computer Simulation of Liquids* (Clarendon, Oxford, 1989).
[47] J.H. Dymond and E.B. Smith, *The Virial Coefficients of Pure Gases and Mixtures* (Oxford University Press, Oxford, 1980).
[48] N. Corbin, W.J. Meath, and A.R. Allnatt, Mol. Phys. **53**, 225 (1984).
[49] R.L. Mills and A.F. Schuch, Phys. Rev. Lett. **23**, 1154 (1969).
[50] A.F. Schuch and R.L. Mills, J. Chem. Phys. **52**, 6000 (1970).
[51] J.C. Raich and R.M. Mills, J. Chem. Phys. **55**, 1811 (1971).
[52] D. van der Spoel, R. van Drunen, and H.J.C. Berendsen, GROMACS User Manual, Biomos BV, Groningen, The Netherlands (unpublished).
[53] H.J.C. Berendsen, J.P.M. Postma, W.F. van Gunsteren, A. DiNola, and J.R. Haak, J. Chem. Phys. **81**, 3684 (1984).
[54] P. Egelstaff, Adv. Chem. Phys. **53**, 1 (1983).
[55] P.A. Egelstaff, Faraday Discuss. Chem. Soc. **66**, 7 (1978).
[56] G.S. Devendorf and D. Ben-Amotz, J. Phys. Chem. **97**, 2307 (1993).
[57] Ph. Marteau, J. Obriot, F. Fondere, and B. Guillot, Mol. Phys. **59**, 1305 (1986).
[58] *CRC Handbook of Chemistry and Physics*, 73rd ed., edited by D.R. Lide (Chemical Rubber, Boca Raton, 1992).
[59] R. Sok, Thesis, University of Groningen, 1994.
[60] S.W. de Leeuw, J.W. Perram, and E.R. Smith, Proc. R. Soc. London Ser. A **373**, 27 (1980).
[61] N. Davidson, *Statistical Mechanics* (McGraw-Hill, New York, 1962).
[62] A. van der Avoird, P.E.S. Wormer, and A.P.J. Jansen, J. Chem. Phys. **84**, 1629 (1986).
[63] T.L. Hill, *Statistical Mechanics* (McGraw-Hill, New York, 1956).
[64] J.S. Rowlinson, *Liquids and Liquid Mixtures* (Butterworths, London, 1969).
[65] K. Kitaura and K. Morokuma, Int. J. Quant. Chem. **10**, 325 (1976).
[66] C.A. Swenson, J. Chem. Phys. **23**, 1963 (1955).
[67] K. Krynicki, E.J. Rahkamaa, and J.G. Powles, Mol. Phys. **28**, 853 (1974).